

Time and energy dependent dynamics of the STM tip – graphene system

P. Vancsó^{1,2,a}, G.I. Márk^{1,2}, Ph. Lambin³, C. Hwang^{2,4}, and L.P. Biró^{1,2}

¹ Research Institute for Technical Physics and Materials Science, P.O. Box 49, 1525 Budapest, Hungary

² Korean-Hungarian Joint Laboratory for Nanosciences, P.O. Box 49, 1525 Budapest, Hungary

³ Department of Physics of Matter and Radiations, University of Namur FUNDP, 61, Rue de Bruxelles, 5000 Namur, Belgium

⁴ Center for Advanced Instrumentation, Division of Industrial Metrology, Korea Research Institute of Standards and Science, Yuseong, 305-340 Daejeon, Republic of Korea

Received 10 June 2011 / Received in final form 12 November 2011

Published online 26 April 2012 – © EDP Sciences, Società Italiana di Fisica, Springer-Verlag 2012

Abstract. Probability current and probability density of wave packets was calculated by solving the three dimensional time-dependent Schrödinger equation for a local potential model of the scanning tunneling microscope (STM) tip – graphene system. Geometrical and electronic structure effects of the three dimensional tunneling process are identified by studying three models of increasing complexity: a jellium half space, a narrow jellium sheet, and a local one electron pseudopotential. It was found that some of the key characteristics of the STM tip – graphene tunneling process are already present at the simple jellium models. In the STM tip – jellium half space system the direction of the momentum does not change during the tunneling event, hence this setup is characterised by introducing an effective distance. For the STM tip – narrow jellium sheet system the direction of the momentum is changed from vertical to horizontal during the tunneling event. The wave packet preferentially tunnels into the bound state of the jellium sheet. For the atomistic model of the graphene sheet an anisotropic spreading of the wave packet was found for hot electrons. This may open new opportunities to build carbon based nanoelectronic devices.

1 Introduction

Graphene [1], a single layer of graphite, is made out of carbon atoms arranged on a honeycomb lattice. This material has unique electronic properties due to the fact that the charge carriers in graphene follow linear dispersion relations [2] near the Fermi level, as if they were governed by the Dirac equation. The resulting massless Dirac-like quasiparticles give rise to new quantum properties such as the anomalous quantum Hall effect [3], the Klein paradox [4] and the Zitterbewegung [5].

Wave packet dynamics (WPD) is an effective method to study electron propagation in nanostructures [6]. It is well suited for the study of localized systems, gives an insight into the dynamics of the system, and can be efficiently parallelized, allowing to deal with realistic 3D systems even on a PC. The dynamics of the electrons represented by wave packets (WPs) in graphene was investigated with different methods in the last years [7–10]. In these theoretical works the propagation of the Gaussian WP was calculated both analytically and numerically and the results give insight into the details of Zitterbewegung and the quantum revival phenomenon. These calculations were performed for an isolated graphene sheet, with or

without external magnetic field, within the usual Dirac cone approximation. Furthermore all works assumed that the initial WP had a Gaussian spatial distribution on the graphene sheet, but it is obviously an idealization.

In order to model a real experimental situation as well as possible, we did not make any assumptions about the initial shape of the electron WP on graphene. Therefore in our model we injected the WP from a simulated scanning tunneling microscope (STM) tip. The WP subsequently tunnels onto the graphene surface and spreads on it. It is well known from STM theory that the tunneling current is influenced by both the geometry (i.e. the spatial positions of the atoms) and the electronic structure. Formerly we performed a detailed analysis of quantum effects arising purely from the geometry of the system which influence the STM imaging process of carbon nanotubes [11–13]. Time dependent scattering of electronic WPs was calculated on a jellium potential model of the STM junction containing different arrangements of carbon nanotubes and point contacts. Distribution of the probability current and the probability density were derived from the time dependent wave function. The theory allowed us to identify components of pure geometrical origin responsible for characteristic distortions of the STM image of carbon nanotubes. These geometrical effects can be well described within the framework of a jellium potential model.

^a e-mail: vancso@mfa.kfki.hu

In this work we present a detailed description of WP evolution for an STM tip – graphene system taking into account the effects arising from both geometrical and electronic structure origin. The metallic STM tip was simulated with a jellium potential as earlier, and in case of graphene, we compared two approximations: a jellium model and a local one electron pseudopotential [14].

The organization of this paper is as follows. Section 2 gives an outline of the WP dynamical method for calculating the tunnel current and it is explained how relevant physical quantities are calculated from the time dependent wave function. In Section 3 we apply the jellium model, formerly used for STM tip – nanotube – support tunneling situations, for the STM tip – graphene system. In Section 4 we incorporate the band structure effects into the calculation by means of a local one electron pseudopotential. Three distinct cases are examined: (a) STM tunneling into a jellium half space, equivalent to a bulk metal sample; (b) STM tunneling into a thin jellium sheet – a model of a graphene-like layer without atomic structure; and (c) STM tip tunneling into graphene with the atomic structure taken into account. We conclude with remarks in Section 5.

Hartree atomic units are used in all formulas except where explicit units are given. SI units are used, however, in all the figures and numerical data.

2 Methods

2.1 Time evolution operator

In order to investigate the dynamics of the tunneling event from the STM tip to the graphene sample and subsequent charge spreading on graphene, we used the WPD method. This conceptionally simple method contains no perturbative approximation but includes all interference and multiple scattering effects. The $\psi(\vec{r}, t)$ time dependent wave function is computed from the time dependent 3D Schrödinger equation by the split operator Fourier transform method [15,16]. The propagated wave function after a time step Δt can be calculated by applying the time-evolution operator on the WP at any instant t

$$\psi(\vec{r}, t + \Delta t) = e^{-i\mathbf{H}\Delta t}\psi(\vec{r}, t). \quad (1)$$

Within the split operator method the time evolution operator is approximated by

$$e^{-i(\mathbf{K}+\mathbf{V})\Delta t} = e^{-i\mathbf{K}/2\Delta t}e^{-i\mathbf{V}\Delta t}e^{-i\mathbf{K}/2\Delta t} + O(\Delta t^3) \quad (2)$$

where the potential energy propagator is a simple multiplication with $\exp(-iV(\vec{r})\Delta t)$ for local potentials, and the effect of the kinetic energy propagator $\exp(-i\mathbf{K}/2\Delta t)$ is given in k space by multiplying the momentum space wave function $\varphi(\vec{k}, t)$ by $\exp(i|\vec{k}|^2\Delta t/4)$. Using this method the time evolution of the $\psi(\vec{r}, t)$ wave function can be determined from any arbitrary initial wave function $\psi(\vec{r}, t = 0)$. From the time dependent wave function the $\rho(\vec{r}, t) = |\psi(\vec{r}, t)|^2$ probability density and the

$\vec{j}(\vec{r}, t) = \text{Im}(\psi^*\nabla\psi)$ probability current density can be calculated. Plane integration of $\vec{j}(\vec{r}, t)$ along a selected measurement plane gives the probability current $I(t)$ crossing the plane as the function of time, and the tunneling probability is $T = \int_0^\infty I(t)dt$. The time dependent Schrödinger equation gives us the time dependent $\psi(\vec{r}, t)$ wave function, which incorporates the complete information about the dynamics of the quantum system in the time domain. Sometimes it is more useful, however, to study the dynamics in the energy domain. Utilizing the time-energy (t - E) Fourier transform we can switch from the time domain dynamics to the energy domain dynamics [16,17]. Indeed, the time dependent wave function can be written as a sum of the eigenstates:

$$\psi(\vec{r}, t) = \sum_n A_n \psi(\vec{r}, E_n) e^{-iE_n t} \quad (3)$$

where A_n are the complex superposition coefficients. Applying the t - E Fourier transform to this gives

$$\begin{aligned} \psi(\vec{r}, E) &= \int_0^{T_{max}} \psi(\vec{r}, t) w(t) e^{iEt} dt \\ &= \sum_n A_n \psi(\vec{r}, E_n) \delta(E - E_n), \end{aligned} \quad (4)$$

where $w(t)$ is a window function which is used to minimize the effect of the finite T_{max} integration time. From this it is obvious that the t - E Fourier transform provides us the eigenstates of the system. We can easily calculate the energy distribution (spectral distribution) of the WP for any given spatial region by integrating the $\rho(\vec{r}, E) = |\psi(\vec{r}, E)|^2$ energy dependent probability density for that region:

$$P(E) = \int_V \rho(\vec{r}, E) dV. \quad (5)$$

2.2 Potential

Within the framework of the jellium potential description of the STM tip – graphene nanosystem the STM tip is approached by a rotational hyperboloid of 0.5 nm apex radius and 15° aperture angle. The jellium potential value is zero outside the effective surface of the tip and -9.81 eV inside. This value was calculated from the HOPG $E_F = 5$ eV Fermi energy and $W = 4.81$ eV work function. In first approximation the graphene sheet is taken as a jellium sheet of finite thickness. The potential inside the sheet is also -9.81 eV. In the next step of approximation the band structure effects are taken into account by applying a local one electron pseudopotential [14] matching the band structure of the graphene sheet π electrons. The potential has the following form

$$V_{graphene}(\vec{r}) = \sum_{j=1}^N \sum_{i=1}^3 A_i e^{-a_i |\vec{r} - \vec{r}_j|^2} \quad (6)$$

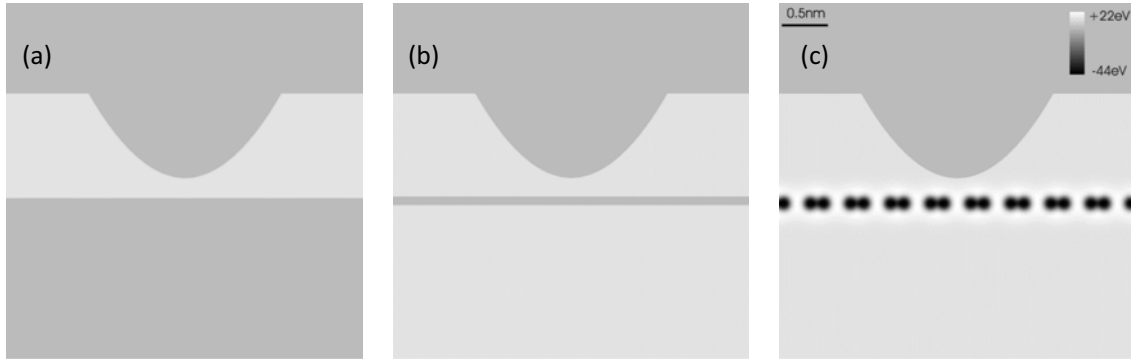


Fig. 1. Grayscale image of the vertical (xz) cross section of the model potentials. (a) Infinite jellium half-plane, (b) thin jellium sheet, (c) graphene pseudopotential. The hyperbolic protrusion on the upper half plane and the horizontal row of black dots (c) represent the vertical cross sections of the tip and graphene, respectively. Black (white) denotes smallest (largest) potential values. The dark gray level is the negative potential inside the STM tip and the jellium sample (-9.81 eV), the light gray level is the vacuum potential (zero).

where \vec{r}_j denote the atomic positions and N is the number of atoms. The A_i , a_i coefficients are given in reference [14]. Figure 1 shows the vertical (xz) cross section of the model potentials of both the jellium and pseudopotential systems (z is the direction perpendicular to the graphene sheet). Absorbing boundary conditions are realized by a drain potential around the presentation box [18]. In order to investigate the tunneling from the STM tip onto the graphene surface, the initial Gaussian WP was launched from the tip bulk towards the apex of the tip with momentum equal to the Fermi momentum: $\vec{k} = (0, 0, -k_F)$. The real space width of the WP is chosen to be $\Delta x, y, z = 0.37$ nm which is considerably larger than the width of the STM tip-graphene tunneling channel 0.1–0.2 nm.

3 Wave packet dynamics results for the jellium model

As we mentioned the tunneling phenomenon is determined by both the geometry and the electronic structure of the system. In order to understand the influence of these factors in the case of the STM – graphene system, first we focused on pure geometrical effects within the jellium potential model. The STM tip – graphene system has two important ingredients: an atomically sharp STM tip and a one atom thick graphene sheet. In order to study the effects of the STM tip and the graphene sheet separately, we compared two different situations, when the STM tip is over a jellium half-space and when the STM tip is above an infinite jellium plane of thickness 0.09 nm (see Fig. 1). Figure 2 shows the time evolution of the probability density in these two cases, Figures 2a and 2b are for the half space, Figures 2c and 2d are for the thin sheet. Figures 2a and 2c are for $t = 1.95$ fs time instant, Figures 2b and 2d are for $t = 3.61$ fs. This two particular time instants were chosen in the moment when the WP already started to tunnel from the tip apex into the sample ($t = 1.95$ fs) and when the WP is already spreading ($t = 3.61$ fs). Majority of the WP is reflected back from the boundary of the tip potential into the tip; note the interference patterns inside the tip; these interferences cause vortices to appear

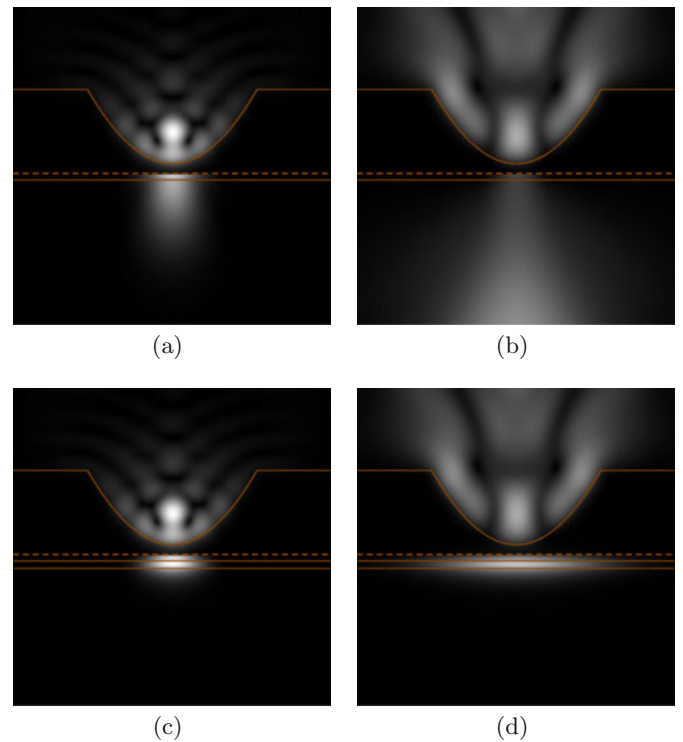


Fig. 2. (Color online) Selected snapshots from the time evolution of the probability density of wave packet shown as grayscale coded 2D sections. (a) and (b) jellium half space. (c) and (d) thin jellium sheet. (a) and (c) $t = 1.95$ fs. (b) and (d) $t = 3.61$ fs. Black corresponds to zero probability. The horizontal dashed line shows the position of the plane, where the tip-sample current was measured. We used a separate grayscale in the tip region and the sample region (above and below the dashed line) because the probability density in the sample is several orders of magnitude smaller than in the tip. The edges of the jellium electrodes are shown by thin lines.

in the probability current density inside the tip. For the case of the half space model, which is “open” on below, the WP can freely propagate in the direction of its initial momentum, in the $-z$ direction. For the case of the thin

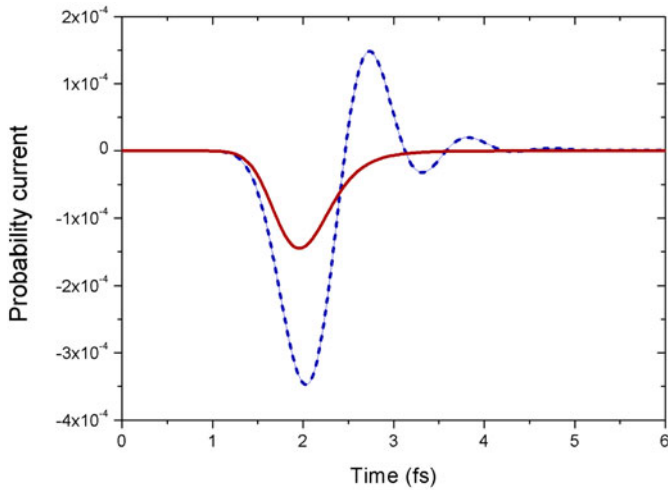


Fig. 3. (Color online) Probability current for the half space jellium (red line) and thin jellium sheet (blue dashed line) models, measured in a plane between the tip and the sample. Negative (positive) values denote current flowing in the $- (+)z$ direction from the tip (sample) into the sample (tip), respectively. Note the back-tunneling into the STM tip in the case of the thin jellium sheet, which is absent at the half infinite jellium model.

jellium sheet model, however, the WP cannot propagate in the $-z$ direction because of the large positive potential step at the lower boundary of the sheet. The WP is thus first accumulated in the jellium sheet below the tip apex and then it begins to spread along the sheet preserving its initial cylindrical symmetry.

The probability current as a function of time (see Fig. 3) was calculated between the STM tip and the sample (the jellium surface) for the two models. In contrast to the jellium half plane where the probability current assumes only negative ($-z$ direction) values, the current assumes negative and positive values as well in the case of the narrow jellium plane. Thus in the second case part of the tunneled WP tunnels back from the jellium surface to the STM tip. A transient period of length $\Delta t \approx 4$ fs can be defined while the probability current still flows between the tip and the surface. Figure 4 shows the transmission probability of the WP for the half space model. The spectral distributions of the WP (Eq. (5)) calculated for the tip and the sample regions are shown at the inset. Due to the fact that the majority of the WP is reflected back into the tip bulk during the transient process, the spectral distribution at the tip region is nearly identical to the initial spectral distribution of the Gaussian WP. The spectral distribution curve for the sample region, however, is shifted towards larger energies. This is because the tunneling process preferentially selects the larger momentum components. To understand better the effect of the tip curvature we compare our computed 3D transmission probabilities of the jellium tip – half space model to a simple plane-plane (1D) model. With the help of the analytical expression for the plane-plane transmission probability an effective tunnel distance [12] d_{eff} can be defined. This

tells us that the barrier consisting of a plane sample and a hyperbolic tip with 0.5 nm radius at 0.32 nm distance is approximately equivalent to a plane-plane barrier with 0.38 nm effective distance.

Figure 5 shows the spectral distribution for the case of the jellium sheet. Note the sharp peak at $E_F + 1.9$ eV. This peak is caused by the bound state of the jellium sheet. Indeed, the jellium sheet has a finite thickness of 0.09 nm and a -9.81 eV depth. This 1D potential well has a bound state at $E = -3.1$ eV. The tunneling event proceeds in two steps. First the WP tunnels into the bound state of the jellium. Then this quasi bound state begins to spread along the sheet. A selection process seems to operate during the transient period in the case of the narrow jellium plane, which means that after the transient process certain components of the WP are found to be tunneled back to STM tip and certain components are found to have remained on the jellium sheet. The oscillatory behaviour of the probability current seen in Figure 4 shows that the transient process is a resonant tunneling process. The inset of Figure 5 shows the radial probability density $\rho(r, E)$ along the jellium sheet. Note that the state at $E_F + 1.9$ eV (corresponding to the bound state) is much more delocalized than the one for E_F . This also proves that these components of the WP near the bound state ($E_F + 1.9$ eV) have a considerably greater probability to spread on the jellium sheet than those near the Fermi energy.

In our jellium calculations the first case (rotational hyperboloid tip and a half infinite bulk sample) is similar to a bulk metallic sample where the WP, after the tunneling event, is able to spread further along the initial direction (z axis) into the sample. The graphene sheet, however, is only one atomic layer thick in the z direction. Our second geometry (STM tip and thin jellium sheet), therefore can be compared to the graphene geometry where the initial WP is not able to spread along the z axis; its momentum has to be changed during the transient process from the vertical (z) into the horizontal (xy) direction.

4 Wave packet dynamics results for the atomistic potential

After discussing the geometrical effects we focus on graphene where the electronic structure is taken into account with a local one-electron pseudopotential (Eq. (6)). Figure 1c shows the values of this potential, for a case when the STM tip is above the centre of a carbon hexagon of the graphene lattice. The details of the time evolution of the WP on the graphene surface (xy cross section) can be seen in Figure 6. As the WP reaches the tip apex from inside the tip bulk, it begins to tunnel onto the central hexagon. Then the WP begins to spread on the graphene sheet along the C-C bonds, in hexagonal symmetry. In this atomic scale process the WP does not “notice” the infinite hexagonal lattice, only follows the pattern of the pseudopotential which has low value channels between the nearest neighbour C-C bonds, and positive values at the

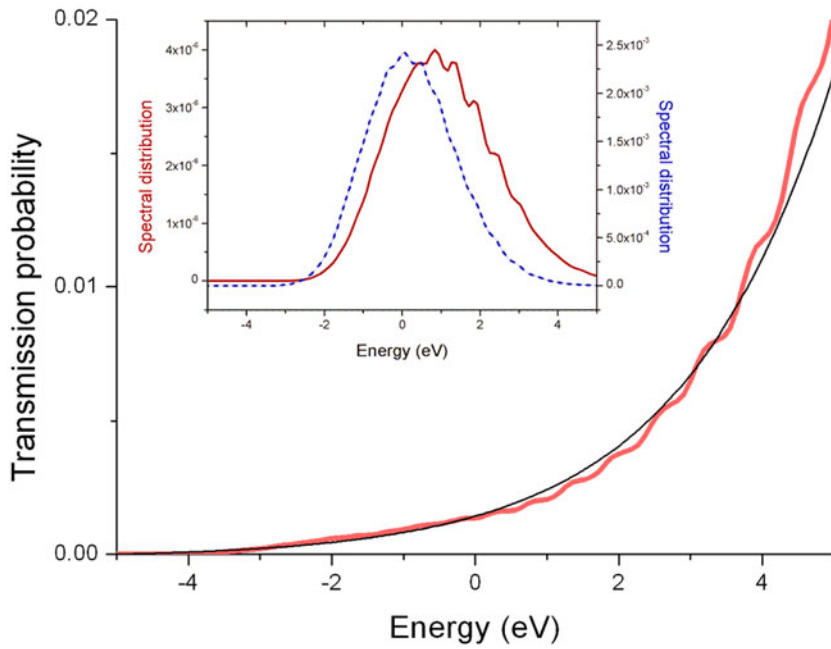


Fig. 4. (Color online) Tip-sample transmission probability for the jellium half space model. As a comparison, the thin back line shows the transmission probability for a plane-plane model (see the text for details). The inset shows the spectral distribution of the wave packet for the sample (red curve) and for the tip (blue dashed curve). Note the different scale of the two functions.

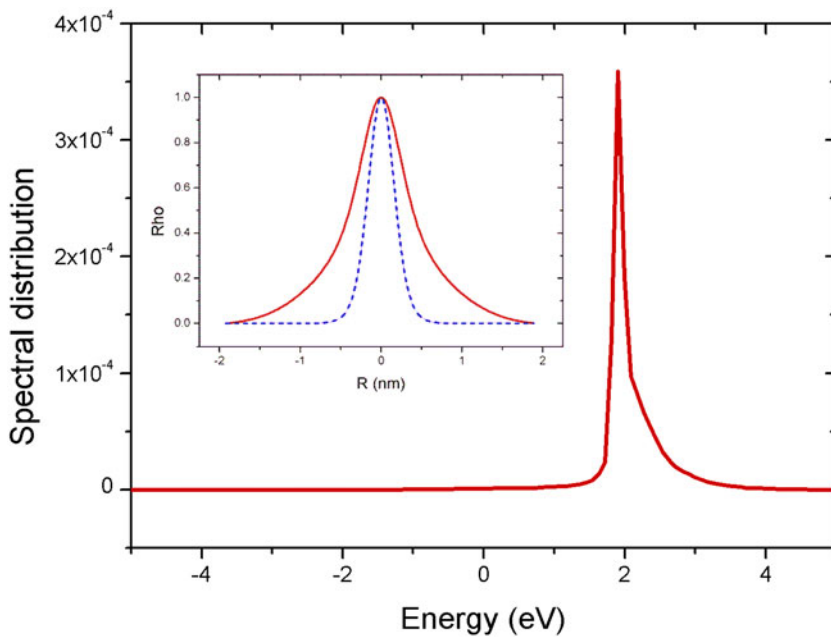


Fig. 5. (Color online) Spectral distribution of the WP calculated for the thin jellium sheet. The inset shows the radial probability density for $E = E_F + 1.9$ eV (red curve) and $E = E_F$ (blue dashed curve). Both functions are normalized to one. Energy is relative to the Fermi energy.

centres of the hexagons. This stage can be regarded as a “molecular” spreading. The direction of the spreading has changed at $t = 3.14$ fs after spreading 1.2 nm from the centre (the point of the graphene sheet below the tip apex). The new propagation direction is matching the zigzag direction of the graphene sheet in direct space which is equivalent to the 6 Γ K directions of the Brillouin-zone. At later times this propagation pattern remains in the time evolution of the probability density. This stage can be regarded as a “solid state” spreading in which the preferential directions are determined by the lattice symmetry. Figure 7 shows the probability current between the STM tip and the graphene surface. As a comparison, we also

show the probability current for the narrow jellium plane model. Both curves show “back and forth tunneling”, i.e. the tunnel current first shows a large negative peak (tunneling towards the sample) then a smaller positive peak (tunneling back into the tip). Hence a momentum selection process (see Sect. 3) is operating in case of both models.

To understand the zigzag propagation directions we calculated the spectral distribution of the WP on the graphene sheet, Figure 8. The large peak at $E = E_F + 3$ eV indicates that “hot” electrons are responsible for the anisotropic spreading on the graphene surface due to the particular band structure. The selection process in this

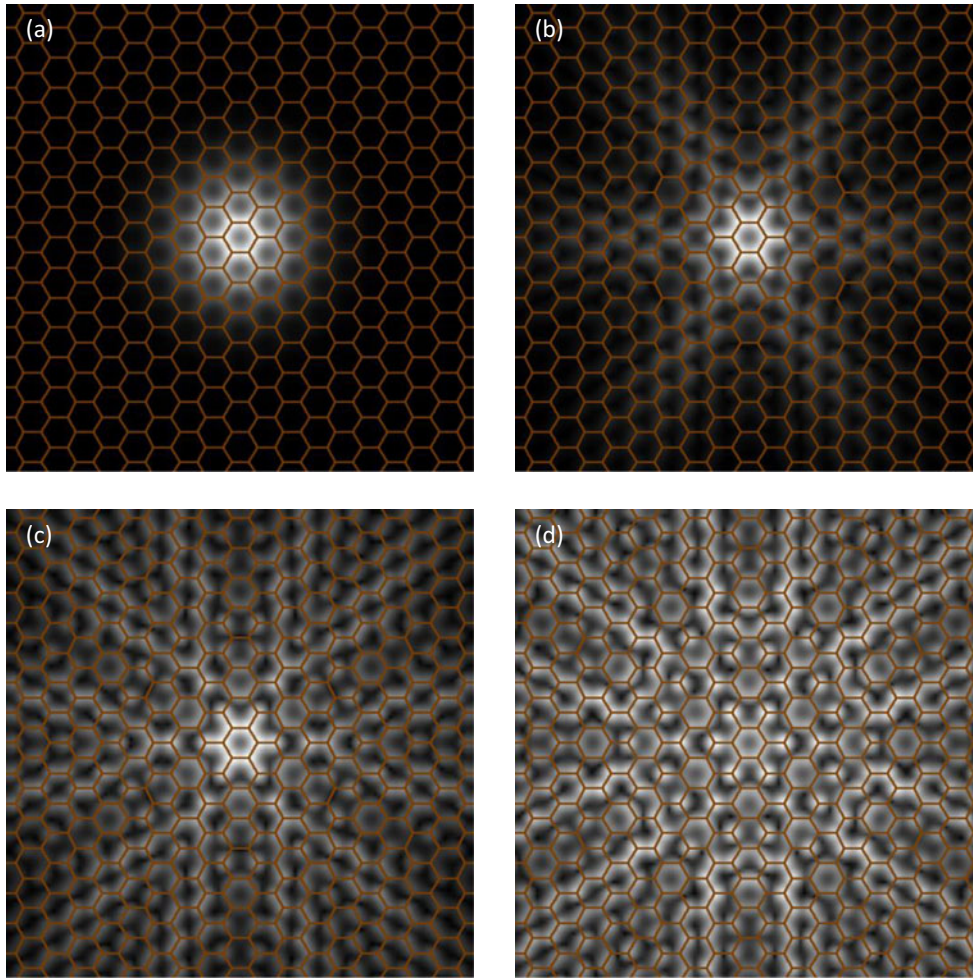


Fig. 6. (Color online) Selected snapshots ($t = 1.50, 2.71, 3.54, 4.29$ fs) from the time evolution of the probability density of the wave packet on the graphene sheet shown as grayscale coded 2D sections. Black corresponds to zero probability. Each image is separately normalized. The graphene network is shown by thin orange lines.

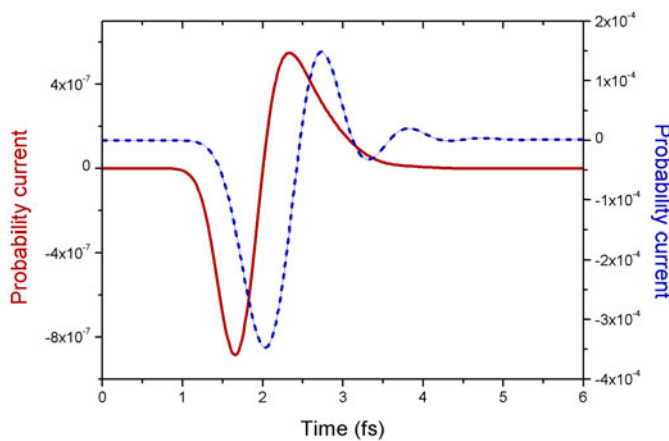


Fig. 7. (Color online) Comparison of the probability current for the jellium and atomistic models of the graphene sheet. Blue dashed curve is for the jellium, red is for the atomistic model. Note the different magnitude of the two currents. Negative (positive) values denote current flowing in the $- (+)z$ direction from the tip (sample) into the sample (tip), respectively.

case is influenced by two factors, a DOS peak and the strongly delocalized states of the system on the graphene at this high energy.

Summarizing the simulation shows an anisotropic in-plane dynamics of the WP following a 60° angular periodicity on the graphene surface. The observed six fold symmetry is seen on the time development of the WP, and the probability current flows in the zigzag directions. This anisotropic charge spreading can be understood from the graphene band structure in the high energy domain, where the isoenergy curves in the graphene dispersion relation are warped into hexagons. The trigonal warping effect becomes enhanced when $E - E_F \approx \gamma$, where $\gamma \approx 2.8$ eV is the tight-binding C-C diagonal matrix element [19]. Due to the band structure and geometrical effects those components are preferred in the transient process which will be spreading in the zigzag directions. Furthermore we can identify two different regimes from the time dependent dynamics on the graphene sheet. At small distances from the tunneling point the molecular physical description dominates, spreading takes place

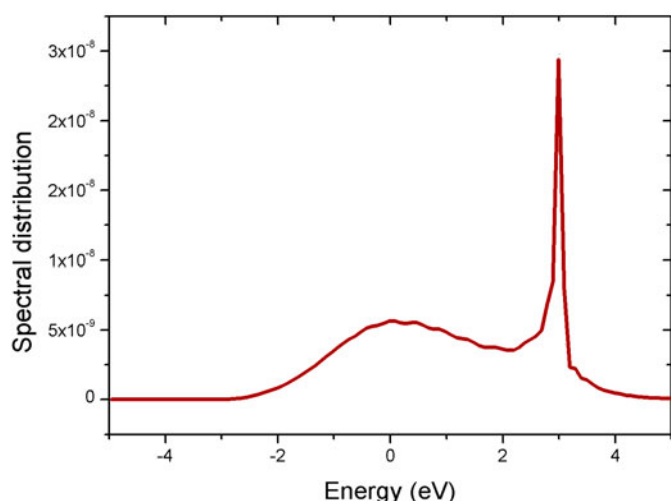


Fig. 8. (Color online) Spectral distribution of the wave packet for the graphene sheet. Note the peak at $E_F + 3$ eV caused by the DOS peak. Energy is relative to the Fermi energy.

along the C-C bonds, at larger distances the solid state physical picture dominates (the zigzag direction determined by the band structure).

5 Conclusion

We performed a detailed analysis of wave packet tunneling for the STM tip – graphene system. We found that several important features of the dynamics are already present at a jellium potential model of the system. Two jellium models were analyzed. In the infinite half space model the wave packet tunnels from the tip into the sample then proceeds in the direction of its original momentum, only the momentum distribution is shifted towards larger energies because the tunneling process preferentially selects the higher energy states. The tunneling process in the thin jellium sheet model differs markedly from this situation, because the wave packet has to change direction from the vertical ($-z$) to horizontal (xy) spreading. If the jellium sheet has a bound state, the wave packet first “fills” this resonant state, and then this state begins to decay. Part of the WP that tunneled onto the sheet tunnels back into the tip due to the localization and another part spreads along the jellium sheet.

To some extent the tunneling event for the atomistic graphene potential proceeds similarly to that for the jellium sheet. The density of states (DOS) of graphene has a peak at $E_F + 3$ eV, the wave packet first tunnels into this state then begins to spread along the graphene sheet. The graphene band structure is anisotropic at this large energy (trigonal warping effect); hence we can observe an anisotropic spreading of the wave packet. The observed sixfold propagation pattern along the zigzag direction combined with the nanopatterning of graphene [20,21] may give new opportunities to build carbon based nano

electronic devices [22]. Indeed, as shown in reference [22], beam splitters, collimators, and beamguides operating in the hot energy region can all be realized by carefully designed hetero-dimensional graphene junctions.

Funding in Hungary by the OTKA-NKTH Grant K 101599 and by the Joint Korean-Hungarian Laboratory for Nanosciences is acknowledged. The Converging Research Center Program through the Ministry of Education, Science and Technology (2010K000980) is acknowledged for funding in Korea. GIM and LPB are grateful to the FNRS in Belgium for financial support in the collaboration with PhL.

References

1. K.S. Novoselov, A.K. Geim, S.V. Morozov, D. Jiang, Y. Zhang, S.V. Dubonos, I.V. Grigorieva, A.A. Firsov, *Science* **306**, 666 (2004)
2. K.S. Novoselov, A.K. Geim, S.V. Morozov, D. Jiang, M.I. Katsnelson, I.V. Grigorieva, S.V. Dubonos, A.A. Firsov, *Nature* **438**, 197 (2005)
3. Y. Zhang, Y.-W. Tan, H.L. Stormer, P. Kim, *Nature* **438**, 201 (2005)
4. M.I. Katsnelson, K.S. Novoselov, A.K. Geim, *Nature Physics* **2**, 620 (2006)
5. M.I. Katsnelson, *Eur. Phys. J. B* **51**, 157 (2006)
6. B.M. Garraway, K.-A. Suominen, *Rep. Prog. Phys.* **58**, 365 (1995)
7. T.M. Rusin, W. Zawadzki, *Phys. Rev. B* **76**, 195439 (2007)
8. G.M. Maksimova, V.Ya. Demikhovskii, E.V. Frolova, *Phys. Rev. B* **78**, 235321 (2008)
9. V. Krueckl, T. Kramer, *New J. Phys.* **11**, 093010 (2009)
10. E. Romera, F. de los Santos, *Phys. Rev. B* **80**, 165416 (2009)
11. G.I. Márk, L.P. Biró, J. Gyulai, *Phys. Rev. B* **58**, 12645 (1998)
12. G.I. Márk, L.P. Biró, J. Gyulai, P.A. Thiry, A.A. Lucas, Ph. Lambin, *Phys. Rev. B* **62**, 2797 (2000)
13. G.I. Márk, L.P. Biró, Ph. Lambin, *Phys. Rev. B* **70**, 115423 (2004)
14. A. Mayer, *Carbon* **42**, 2057 (2004)
15. J.A. Fleck, J.R. Morris, M.D. Feit, *Appl. Phys.* **10**, 129 (1976)
16. M.D. Feit, J.A. Fleck, A. Steiger, *J. Comput. Phys.* **47**, 412 (1982)
17. S.A. Chin, S. Janecek, E. Krotscheck, *Comput. Phys. Commun.* **180**, 1700 (2009)
18. B. Poirier, T. Carrington Jr., *J. Chem. Phys.* **118**, 17 (2003)
19. R. Saito, G. Dresselhaus, M.S. Dresselhaus, *Phys. Rev. B* **61**, 2981 (2000)
20. L. Tapasztó, G. Dobrik, Ph. Lambin, L.P. Biró, *Nature Nanotechnol.* **3**, 397 (2008)
21. P. Nemes-Incze, G. Magda, K. Kamarás, L.P. Biró, *Nano Res.* **3**, 110 (2010)
22. Zh. Wang, F. Liu, *ACS Nano* **4**, 2459 (2010)